Prediction of microtunnelling jacking forces using a probabilistic observational approach

Brian Sheil[1]

[1]Royal Academy of Engineering Research Fellow, Department of Engineering Science, University of Oxford, Parks Road, Oxford OX1 3PJ, UK.

ABSTRACT

Microtunnelling is an increasingly popular means of locating utilities below ground. The ability to predict the total jacking force requirements during a drive is highly desirable for anomaly detection, to ensure the available thrust is not exceeded, and to prevent damage to the pipe string and/or launch shaft. However, prediction of the total jacking force is complicated by site geology, the use of a lubricated overcut, work stoppages, tunnel boring machine driving style and pipe misalignment. This paper introduces a probabilistic observational approach for forecasting jacking forces during microtunnelling. Gaussian process regression is adopted for this purpose which allows forecasts to be performed within a probabilistic framework. The proposed approach is applied to two recent UK microtunnelling monitoring projects and the forecasts are appraised through comparisons to predictions determined using design methods currently applied in industry. The results show that the proposed framework provides excellent forecasts of the monitored field data and highlights a significant opportunity to complement existing prescriptive design methods with probabilistic forecasting techniques.

INTRODUCTION

There is a vast network of buried infrastructure and services in the UK extending to well over 1.5 million km comprising water, sewer, gas and electricity. To keep pace with growing populations and to meet future infrastructure demands, a substantial amount of construction work on buried infrastructure is required (Royston et al. 2020a, 2020b). Relative to traditional open-cut construction, microtunnelling is an increasingly popular means of locating utilities below ground due to the reduction in costs, noise and air pollution, and impact on the surrounding infrastructure and environment (Phillips et al. 2019).

Long-distance drives, often with curves, are desirable in the industry to avoid costly intermediate shafts and provide a greater range of solutions for accommodating surface disruptions in sensitive areas (Bergeson 2014). One of the greatest risks in long-drive microtunnelling is the development of excessive soil-structure penetration resistances, to the point where they exceed the total available jacking thrust. Prediction of the total jacking force is also complicated by site geology, the use of a lubricated overcut, work stoppages, tunnel boring machine (TBM) driving style and pipe misalignment (Meskele and Stuedlein 2015, Cheng et al. 2017, Sun et al. 2019). This does not lend itself easily to simplification through theoretical relationships or numerical modelling. Instead, site engineers rely on a combination of empiricism from experience on site and ad hoc theoretical relationships which have not been rigorously validated.

The proliferation of data collected by modern TBMs presents a substantial opportunity for the application of data analysis and pattern recognition techniques to support the decision-making process on site with timely and meaningful information (Shen et al. 2016, Sheil et al. 2020a). Originally proposed by Peck (1969), the observational method is an acceptable verification method for limit states in Eurocode 7 and is now well-established in geotechnical engineering (Spross and Johansson 2017). Data-driven modelling and forecasting has quickly developed into an essential tool in a broad range of practical domains including seismology (e.g. Holliday et al. 2005), healthcare (e.g. Reis and Mandl, 2003) and financial markets (e.g. Kim 2003). These approaches advance the traditional observational method by employing machine learning systems, predicated

on the assumption of the presence of a sufficient amount of data to describe the modelled system's physics.

This paper describes the development of a probabilistic observational approach for the prediction of jacking forces during microtunnelling. Gaussian process (GP) regression is adopted for this purpose which allows forecasts to be performed within a probabilistic framework. This allows a project-specific approach to be adopted in which a GP is automatically constructed using data from each individual project. The proposed approach is applied to two recent UK microtunnelling monitoring projects and the forecasts are appraised through comparisons to predictions determined using design methods currently applied in industry.

BACKGROUND: FACTORS INFLUENCING MICROTUNNELLING JACKING FORCES

Accurate forecasting of the total jacking force requirements for microtunnelling drives is desirable to (a) develop a model of 'normality' from which anomalous observations can be inferred (short-term), (b) inform (expensive) inter-jack installation ('medium'-term), and (c) predict maximum likely jacking to avoid damage to the shaft and / or pipe string (long-term). The total jacking force, F_T, is composed of the TBM face resistance, F_0, and the soil-structure frictional resistance, F_s, acting along the length of the pipe string. For long drives, F_T is almost entirely governed by F_s and the adopted pipe-soil lubrication system becomes a key factor in the development of jacking forces. Lubrication during microtunnelling serves three main purposes: (a) stabilisation of the tunnel bore, (b) flotation of the pipe string, and (c) reduction of the pipe-soil interface friction coefficient (Milligan and Marshall 1998). Based on nine monitored microtunnelling drives, Pellet-Beaucour and Kastner (2002) observed that the use of lubricants can reduce frictional stresses by anywhere between 50% and 90%. From a field monitoring case study, Shi et al. (2018) presented significantly lower interface friction coefficients for a lubricated steel-soil interface compared to values documented in the literature relating to concrete pipes. From a back-analysis of two drives in silty sand, O'Dwyer et al. (2018) noted that lubrication was very effective at maintaining low skin friction levels, and that the pipe string was almost fully buoyant for the majority of the drive.

Work stoppages also have a considerable influence on F_s where a peak in jacking force is typically observed upon resumption of tunneling (Cheng et al. 2017). Stoppages on site can vary in duration from < 30 mins for pipe changes to between 12 and 48 hours for overnight and weekend stoppages respectively. However, a general consensus has yet to be reached in the literature as to the primary cause. Norris and Milligan (1992) suggested that these increases in jacking forces are attributable to differences in shearing rates in cohesive soils. Pellet-Beaucour and Kastner (2002) postulated that these effects are related to differences in dynamic and static friction coefficients. More recently, O'Dwyer et al. (2019) concluded that jacking force increases following a stoppage were largely governed by the stoppage duration, suggesting that these effects are instead a consolidation phenomenon.

While our understanding of these factors have improved greatly over the past thirty years, the literature contains many examples where prescriptive design methods fail to provide satisfactory prediction of field behaviour. Norris and Milligan (1992) used instrumented pipe sections on five construction projects to measure pipe-soil contact stresses. The measured contact stresses were highly-localised and proved difficult to capture with theoretical relationships. Chapman and Ichioka (1999) reported that one of the main obstacles to an accurate estimation of pipe jacking forces is the inherent variability of the construction operation itself. Those authors noted that closed-form design approaches are not capable of predicting fluctuations in jacking force that arise from site-specific variations. Milligan and Norris (1999) reported that jacking force fluctuations are often due to unanticipated pipe / TBM misalignments. Rahjoo et al. (2012) documented significant incongruities when jacking forces measured in the field were compared to predictions determined using a range of published empirical models. Similarly, Reilly and Orr (2012) noted that existing design methods provided poor predictions of jacking forces measured during drives in coarse-grained soils. Choo and Ong (2015) applied site-specific direct shear results to well-established empirical models for the prediction of jacking forces. Although good agreement was observed, the models were only capable of predicting the average jacking force and not variations due to stoppages. Even in rock, where the tunnel bore can be assumed stable, Barla et al. (2006) and Sheil et al. (2016) have attested to the difficulty in predicting jacking forces. These investigations

highlight the poor track record of closed-form design methods in this area and provides significant motivation for the consideration of a complementary data-driven approach.

FIELD MONITORING

Overview

Tunnelling and lubrication data from two drives, 'Drive A' and 'Drive B', in Blackpool, UK are considered in this paper (shown in Fig. 1). A total drive length of 295 m and 272 m was measured for Drives A and B respectively. Drive A had an initial launch invert depth of 7.59 m below ground level (BGL) and a cover depth which varied between 6.2 m and 7.8 m. Drive B had an initial launch invert depth of 7.61 m BGL and a cover depth which varied between 5.2 m and 6.3 m. The slurry shield TBM (Herrenknecht AVN 1200) had a cutterhead diameter, D_c, of 1515 mm whereas each concrete pipe had an outer diameter, D_p, of 1490 mm. This created a 25 mm 'overcut' into which lubricant was pumped. The length and mass of each pipe was 2.5 m and 3660 kg respectively.

A bentonite solution was adopted for the lubrication comprising Hydraul-EZ and water in the ratio 1:18 (by weight) with minor additions of MX polymer, torque reducer and soda ash. Bentonite stations were located on every fifth pipe along the string with the first station located directly behind the TBM. Each station comprised three lubrication ports, trisecting the pipe circumference, and were positioned midway along the length of the pipe. The bentonite system used by these TBMs are volume-controlled, calculated from the TBM advance rate and ground conditions.

Ground conditions

The locations of three boreholes (BH1, BH2 and BH3) in relation to the line of Drives A and B are shown on Fig. 1. The ground conditions are summarised in Fig. 2 and comprise made ground (0.4 m thickness) underlain by gravelly sand (2.6 m - 4.4 m), peat (1.0 m - 1.7 m), silt (1.2 m - 2.5 m) and silty sand/sand (>5.0 m). Tunnelling occurred predominantly in the silt and silty sand layers. The water table was located 1.2 m below ground level. Uncorrected Standard Penetration Test (N) values are also shown in Fig. 2. An average N1 value (N values corrected for overburden

pressure) was used to derive an operational friction angle for the material above the tunnel crown using correlations proposed by Stroud (1989). This exercise yielded a friction angle of approximately 32°. The reader is referred to O' Dwyer et al. (2018, 2019) for additional details on the project.

Monitored results: structure of jacking force data

The output data from the TBM was recorded at 200 mm intervals of jacked distance. Due to a technical issue with the data acquisition system, data for Drive A were only recorded beyond a jacked distance of 62 m. The development of total jacking force with jacked distance is shown in Figs 3(a) and 3(b) for Drives A and B respectively. From both figures, it can be seen that the data contains a number of important 'features' that are desirable to capture within a data-driven approach: (a) a global linear trend representing an increase in frictional resistance with jacked distance, (b) occasional, discontinuous and transient peaks representing the influence of stoppages and (c) minor fluctuations arising from miscellaneous site factors such as pipe misalignments and TBM driving style.

GAUSSIAN PROCESSES

Gaussian Process regression

A GP is a stochastic method involving a collection of random variables of which any finite number follow a joint Gaussian distribution (Rasmussen and Williams, 2006). GPs provide a method to perform Bayesian inference about functions in a non-parametric way. One of the key aspects of GPs is the use of covariance functions (also known as 'kernels') which encodes prior assumptions about the functions one wishes to learn (in this case the monitored data). This avoids reliance on algebraic mapping between inputs and outputs. The overall aim of the process is to learn a regression model of the form $y = f(x) + \epsilon$, where $f(x)$ is a latent function representing the underlying structure of the data and $\epsilon \sim (0, \sigma^2)$ is a noise term where σ^2 is the variance of the noise. Given training dependent function values $\mathbf{Y} = \{y_1, y_2, \ldots, y_n\}$ evaluated at locations $\mathbf{X} = \{x_1, x_2, \ldots, x_n\}$, the

objective is to obtain the value of the predictand $\mathbf{Y}^* = \{y^*_1, y^*_{2,\ldots,} y^*_m\}$ at known values of $\mathbf{X}^* = \{x^*_1, x^*_{2,\ldots,} x^*_m\}$. A Gaussian distribution can be completely described by a mean vector, μ(x), and covariance function $k(x,x')$ of input pairs x and x′ to describe an underlying real process f(x) as follows:

$$\mu(x) = \mathbb{E}[f(x)] \tag{1}$$

$$k(x, x') = \mathbb{E}\left[\big(f(x) - \mu(x)\big)\big(f(x') - \mu(x')\big)^{\mathrm{T}}\right] \tag{2}$$

The GP can therefore be defined as:

$$f(x) \sim \mathcal{GP}(\mu(x), k(x, x')) \tag{3}$$

where the symbol '~' means 'distributed according to'. In this study, noise terms are added to the diagonal of the covariance matrix, to account for noisy observations. This is equivalent to adding a covariance function of the following form:

$$k(x_i, x_j) = \delta_{i,j}\sigma^2 \tag{4}$$

where $\delta_{i,j}$ is the Kronecker delta function. Parameters of the covariance functions, referred to as hyperparameters, define the exact form of the function and are inferred by training on the observed monitored data. The likelihood of the observed data can be estimated by marginalising over the latent function **f**:

$$p(\mathbf{Y}|\mathbf{X}) = \int_{\mathbf{f}} p(\mathbf{Y}|\mathbf{f}, \mathbf{X}) p(\mathbf{f}|\mathbf{X}) d\mathbf{f} \tag{5}$$

The process of learning hyperparameters, θ, from data is achieved using an empirical Bayes approach by maximising the log likelihood function:

$$\log p(\mathbf{y}|\mathbf{X}, \theta) = -\frac{1}{2}\log\left|\mathbf{K}_{\mathbf{x},\mathbf{x}} + \boldsymbol{\sigma}^{\mathbf{2}}\mathbf{I}\right| - \frac{1}{2}\mathbf{Y}^{\mathrm{T}}[\boldsymbol{K}_{\mathbf{x},\mathbf{x}} + \boldsymbol{\sigma}^{\mathbf{2}}\mathbf{I}]^{-1}\mathbf{Y} - \frac{n}{2}\log(2\pi) \tag{6}$$

where ***I*** is the identity matrix, *n* is the number of training cases and $\boldsymbol{K}_{\mathbf{x},\mathbf{x}}$ denotes the covariance matrix. This process incorporates a trade-off between model fit and complexity. A Bayesian formulation can subsequently be adopted to forecast the function outputs **f*** at inputs **X***, having

observed **Y** (a noisy observation of the underlying function **f**) corresponding to **X**. The joint probability of **Y** and **f*** that is conditional on **X** and **X*** can be obtained as follows:

$$p\left(\begin{bmatrix}\mathbf{y}\\ \mathbf{f}^*\end{bmatrix}\right) = N\left(\begin{bmatrix}\mathbf{y}\\ \mathbf{f}^*\end{bmatrix}\middle|\begin{bmatrix}\boldsymbol{\mu}\\ \boldsymbol{\mu}^*\end{bmatrix}, \begin{bmatrix}\boldsymbol{K}+\boldsymbol{\sigma}^2\mathbf{I} & \boldsymbol{K}_{\mathbf{x},\mathbf{x}^*}\\ \boldsymbol{K}_{\mathbf{x},\mathbf{x}^*}^{\boldsymbol{T}} & \boldsymbol{K}_{\mathbf{x}^*,\mathbf{x}^*}\end{bmatrix}\right) \quad (7)$$

The posterior predictive density of **f*,** conditioned on the observed monitored data, can finally be defined as:

$$p(\mathbf{f}^*|\mathbf{X}^*,\mathbf{X},\mathbf{Y}) = N(\mathbf{M}^*,\boldsymbol{\Sigma}^*)$$

$$\mathbf{M}^* = \boldsymbol{K}_{\mathbf{x},\mathbf{x}^*}^{\boldsymbol{T}}\left[\boldsymbol{K}_{\mathbf{x},\mathbf{x}}+\boldsymbol{\sigma}^2\mathbf{I}\right]^{-1}\mathbf{Y} \quad (8)$$

$$\boldsymbol{\Sigma}^* = \boldsymbol{K}_{\mathbf{x}^*,\mathbf{x}^*} - \boldsymbol{K}_{\mathbf{x},\mathbf{x}^*}^{\boldsymbol{T}}\left[\boldsymbol{K}_{\mathbf{x},\mathbf{x}}+\boldsymbol{\sigma}^2\mathbf{I}\right]^{-1}\boldsymbol{K}_{\mathbf{x},\mathbf{x}^*}$$

Covariance functions

The 'core' covariance functions adopted for this study are defined in Table 1 and include linear, periodic, squared exponential, Matérn 5/2 and Matérn 3/2 functions. The structure of each core covariance function is illustrated in Fig. 4. The linear covariance function, k_{LIN}, is non-stationary and can be obtained from linear regression. The periodic covariance function, k_{PER}, is a stationary covariance function that enables modelling of periodic functions. It is parameterised by a length-scale *l* and periodicity parameter, *p*. The squared exponential covariance function, k_{SE}, (often referred to as the radial basis function) is a stationary and infinitely differentiable covariance function parameterised by a length-scale parameter *l*. Finally, the Matérn class of covariance functions are stationary and represent a generalisation of k_{SE} (Matérn 1960). These covariance functions are parameterised by a length-scale parameter *l*. An additional parameter v controls the smoothness of the learned function but is not optimised based on the training data, unlike *l*. For v = ∞, the covariance function is equivalent to k_{SE}. Popular intermediate values used here are v = 5/2 (twice differentiable) and v = 3/2 (once differentiable). The influence of v on the structure of a sample drawn from a GP is qualitatively illustrated in Fig. 5.

These core covariance functions can be combined (summation, multiplication etc.) to create customized covariance functions to model complex processes. This is because the direct sum and

the tensor product of multiple covariance functions are also covariance functions. For example, while k_{PER} corresponds to an exact periodic structure, $k_{LIN+PER} = k_{LIN} + k_{PER}$ corresponds to a periodic structure with a global linear trend (see Fig. 6). In this study, only covariance function summation is considered as this has been shown to be sufficiently capable of capturing complex data structures (Duvenaud, 2014). By summing covariance functions, the data is modelled as a superposition of independent functions representing different structures present in the data shown in Fig. 3. All possible pairs of the core covariance functions in Table 1 were considered for analysis. Recognising that the summation of two linear covariance functions yields the same result as a single linear covariance function, this leaves a total of 19 combinations to be assessed. For this work, the GP models were developed using Scikit−Learn (Pedregosa et al., 2011) within Python 3.6.

GP FORECASTING: IMPLEMENTATION

The implementation of the proposed approach is illustrated in Fig. 7. Filtering feature selection, using the Pearson correlation matrix technique, was adopted to identify the most discriminant parameters recorded by the TBM for the prediction of total jacking force. As a result of this process, TBM records of time and jacked distance are used as the GP model inputs whereas total jacking force represents the model output. During training, the GP model autonomously develops a relationship between jacked distance, time (and tacitly penetration rate, stoppage duration) and total jacking force within a probabilistic framework. Gaussian process training and forecasting is performed using a sliding window approach. The forecast origin is defined as the last point of the known (monitored) value from which the GP forecast is to be performed. The forecast horizon, h, is the number of steps into the future for which the forecasts are to be performed. The GP model is retrained and forecasts are performed by sequentially moving newly-acquired data to the training set, as shown in Fig. 8(a) for a fixed forecast horizon and Fig. 8(b) for ‘long-term forecasting’. If the size of the training dataset exceeds a maximum size, r, then the oldest datapoint is discarded.

In this work, a 100(1-α)% prediction interval (PI) is adopted:

$$PI_{t+1} = \hat{y}_{t+1} \pm t_{\alpha/2,n-n_p} \times s \times \sqrt{h} \quad (9)$$

where $\hat{y}_{t+1}$ denotes the forecast for step $t + 1$ made at step t, $t_{\alpha/2,n-np}$ is the $\alpha/2$ quantile of a t-distribution with $n - n_p$ degrees of freedom, n_p is the number of parameters in the model and s is the square root of the mean of the squared prediction residuals in the training dataset. In this paper, a significance level of 1% ($\alpha = 0.01$) is initially adopted as default to ensure all peaks in jacking force are captured. The root mean squared error (RMSE) is used to define the error between the mean GP forecast and the monitored data as follows:

$$\text{RMSE} = \sqrt{\frac{1}{k}\sum_{i=1}^{k}\left(f_i^* - y_i^*\right)^2} \quad (10)$$

where k is the total number of forecasts made. In all cases, the forecast accuracy is computed by averaging over the test sets.

FORECASTING RESULTS: DRIVE A

Influence of GP covariance function

Fig. 9 shows the results of the GP forecasting, using the RMSE defined in equation (10), for all 19 instances of the covariance function and for four different forecast horizons: h = 1 (0.2 m; 'short-term'), h = 12 and 50 (2.4 m, approximately one pipe length, and 10 m; 'medium-term'), and long-term (variable h). The short- and medium-term forecasting was performed using the approach outlined in Fig. 8(a) whereas the long-term forecasting used the approach outlined in Fig. 8(b). In these initial analyses, no maximum has been imposed on the size of the training dataset i.e. $r = \infty$.

It can be observed that short-term forecasts of the total jacking force determined using the linear covariance function, k_{LIN}, are the least accurate. This is because the simplified structure of this covariance function is not capable of capturing the complex relationship between jacked distance, time and force (henceforth referred to as the 'distance-time-force relationship'). Conversely, the best short-term forecast accuracy is achieved using the $k_{MAT3+MAT5}$ covariance function. Interestingly, the performance of the covariance functions appears to be most closely linked to the

function's 'smoothness', controlled by v, where k_{Mat3} (v = 3/2) provides the best forecast accuracy, followed by k_{Mat5} (v = 5/2) and k_{SE} (v = ∞). This finding is perhaps more obvious when the structure of the monitored data presented in Fig. 3 is compared with those of the covariance functions in Fig. 5.

With the exception of long-term forecasts performed using covariance functions comprising a periodic element, an increase in *h* causes a deterioration in forecast accuracy. This is because the uncertainty of a forecast increases in proportion to *h*. For greater forecast horizons, covariance functions comprising k_{LIN} generate the most accurate GP forecasts because of its simple structure and independence of a length-scale parameter, *l*. In general, it is not possible to accurately extrapolate more than *l* units away from the origin. As variations in the monitored data occur over short intervals of jacked distance, the optimised values of *l* are low and therefore forecasts quickly return to the mean of the prior. This leads to a deterioration in the accuracy of forecasts generated using covariance functions comprising a length-scale dependency for greater forecast horizons.

Forecasts of the development of the total jacking force with jacked distance determined using the most accurate GP covariance functions are plotted in Fig. 10 for short- and medium-term forecasting and for $r = \infty$. In these plots, a solid line is used to denote the GP best-estimate whereas a shaded region denotes the 99% PI defined by equation (9). From Fig. 10(a), the structure of the data, particularly stoppage-induced peaks in jacking force, appear to be well-captured by the $k_{MAT3+MAT5}$ GP where all peaks are encapsulated by the 99% PI. This highlights the ability of the GP model to automatically establish a site-specific probabilistic relationship between stoppage time and jacking force. Similar observations can be drawn from the results presented in Figs. 10(b) and 10(c) using k_{LIN+SE} and k_{LIN} respectively. In this case, the 99% PI is larger due to forecasting h = 12 and 50 steps ahead respectively. While there is a deterioration in the agreement between the GP best-estimates and the monitored data, the 99% PI provides a safe estimate of the maximum total jacking force.

Long-term GP forecasts using the most accurate covariance function (in this case k_{LIN}) is shown in Fig. 11 for three arbitrary instances of the forecast origin. The much greater forecast horizon causes a significant increase in the uncertainty of the forecasts and therefore also the 99% PI.

While there is a clear deterioration in the fidelity of the GP's forecast of the distance-time-force relationship, the GP provides excellent forecasts of the linear friction trend in all instances.

Influence of maximum training window size

Application of the proposed approach necessitates the inversion of an $n \times n$ matrix which may become computationally demanding for large training datasets i.e. for long drives (c.f. equation (8)). Fig. 12 explores a 'computationally light' implementation of the proposed approach by imposing a maximum size, r, on the training dataset where all four forecast horizons have again been considered. In this case, the RMSE has been normalised by the corresponding $r = \infty$ value (i.e. no maximum has been imposed). Intuitively, a reduction in r causes a gradual increase in forecast error because there is an insufficient amount of data to accurately describe the distance-time-force relationship. The results also suggest that long-term forecasting requires more data to reliably capture the long-term friction trend. By way of example, short- and medium-term forecasts determined using the extreme case of r = 2.4 m (approximately one pipe length) are presented in Fig. 13. It can be seen that insufficient training data causes the GP to provide poor predictions of stoppage-induced peaks in jacking force. Nevertheless, the results in Fig. 12 show that the selection of 'intermediate' values of r allows the proposed approach to be optimised for real-time implementation for a modest trade-off in the forecast accuracy; these 'optimal' values are presented in Table 2 and were determined based on computational time and forecast accuracy.

Influence of prediction interval

While the previous results highlight the ability of the proposed GP model to provide a 'best-estimate' of the total jacking force, it is more common for a safe 'upper bound' estimate to be used in design. Rather than using a single upper bound estimate, the GP model provides an expedient approach to derive a probabilistic upper bound. To this end, Figs. 14 and 15 plot GP forecasts for various forecast horizons using the optimal parameters presented in Table 2. Three prediction intervals have been considered for these comparisons: 99%, 90% and, as an extreme case, 50%.

It can be seen that for short-term forecasting, the prediction intervals are tightly-banded given the high level of certainty in the forecasts (see Fig. 14(a)). In this case a PI = 99% is necessary to capture all peaks in jacking force. An increase in *h* to 12 and 50 causes an increase in the range of the prediction intervals as shown in Figs. 14(b) and 14(c) respectively. While a 99% PI provides an appropriate upper bound forecast for *h* = 1 and 12, it provides a conservative estimate of the upper bound in Fig. 14(c); in this instance PI = 90% is sufficient. Similar findings may be deduced from Fig. 15 where it can be seen that the PI = 99% and 90% appear overly-conservative because of the large forecast horizon. The proposed methodology therefore allows the engineer the flexibility to develop an upper bound envelope of the jacking force corresponding to a desired risk level.

VALIDATION OF PROPOSED APPROACH: DRIVE B

Existing jacking force design methods

To validate the proposed methodology, forecasts of Drive B are compared to predictions determined using existing design guidelines commonly used in industry. The Pipe Jacking Association (PJA 1995) design guidance recommends that the face resistance, F_0, is taken to be at least the total horizontal stress, σ_h, acting on the cutterhead face:

$$F_0 = \sigma_h \frac{\pi D_c^2}{4} \tag{11}$$

The frictional resistance acting on the pipe string in cohesionless soils is defined as follows:

$$F_s = \frac{\pi D_c}{2}(\sigma'_v + \sigma'_h)\tan\delta \cdot L \tag{12}$$

$$\sigma'_v = \frac{\gamma B}{K\tan\phi'}\left(1 - e^{-\frac{K\tan\phi' z_w}{B}}\right)e^{-\frac{K\tan\phi'(H-z_w)}{B}} + \frac{\gamma' B}{K\tan\phi'}\left(1 - e^{-\frac{K\tan\phi'(H-z_w)}{B}}\right) \tag{13}$$

$$\sigma'_h = K(\sigma'_v + 0.5\gamma' D_c) \tag{14}$$

$$B = \frac{D_c}{2}\tan\left(45° - \frac{\phi'}{2}\right) + \frac{D_c}{2\sin\left(45° + \frac{\phi'}{2}\right)} \tag{15}$$

$$K = \frac{1 - \sin\phi'}{1 + \sin\phi'}$$

where σ'_v and σ'_h are the vertical and horizontal effective soil stresses respectively, δ is the pipe-soil interface friction angle, L is the current drive length, z_w is the depth of the water level below the ground surface, γ and γ' are the total and effective soil unit weights respectively, K is the coefficient of lateral earth pressure and H is the cover depth measured from the tunnel crown. The recommended interface friction angle for a concrete pipe in cohesionless soil is $0.7\phi' < \delta < 0.9\phi'$ (PJA 1995); a value of $\delta = 0.8\phi'$ has therefore been adopted. The influence of stoppages is accounted for by augmenting the value of F_s determined using equation (12) by 50% (PJA 1995).

More recently, Staheli (2006) proposed an alternative expression for F_s:

$$F_s = \frac{\mu_r \cdot \gamma \cdot D_p \cdot \cos\left(45° + \frac{\phi'_r}{2}\right)}{2 \cdot \tan\phi'_r} \cdot \pi \cdot D_p \cdot L \tag{16}$$

where μ_r and ϕ'_r are the residual interface friction coefficient and residual soil friction angle respectively. In this case, the widely adopted relationship for μ_r for microtunnelling operations has been adopted (Japan Microtunnelling Association 2000; Pellet-Beacour and Kastner 2002; Sofianos et al. 2004; Staheli 2006; Shou et al. 2010):

$$\mu_r = \tan\left(\frac{\phi'}{2}\right) \tag{17}$$

Instead of a prescriptive design method, the Concrete Pipe Association of Australasia (CPAA 2013) present typical values for the jacking resistance per unit area of the external surface of the pipe string, as shown in Table 3. These guidelines also recommend an additional 20-50% to account for stoppage-induced increases in jacking force (50% has again been adopted here).

Application: forecasting Drive B jacking forces

For the GP forecasts of Drive B, the optimal parameters presented in Table 2 have been adopted. Also superimposed on these plots are the predictions determined using the PJA (1995), Staheli (2006) and CPAA (2013) design methods. The shaded region associated with the PJA (1995) and

CPAA (2013) predictions represent the recommended additional 50% increase in jacking force to account for stoppage-induced peaks. The results presented in Fig. 16 show that the 99% PI provides a very good upper bound estimate of the maximum jacking forces for all three forecast horizons. Conversely, the jacking forces are significantly over-predicted by the existing prescriptive design methods. This is likely due to an over-prediction of both the coefficient of friction for lubricated interfaces and the normal soil stresses exerted on the pipe string. This reflects the effectiveness of modern lubrication systems in reducing friction during microtunnelling and suggests that the use of historical pipe jacking parameters may provide overly conservative predictions.

Similar conclusions can be drawn from an examination of the long-term forecasting results presented in Fig. 17. In this case, the 99% PI estimate appears overly-conservative and even a 50% prediction interval appears to provide a safe envelope. Nevertheless, all three bounds represent an improvement on the predictions determined using the existing design methods. The traditional design methods correspond to less than a 50% prediction interval during the initial stages of the drive (see Fig. 17(a)) whereas they significantly exceed a 99% prediction interval as the drive progresses (see Fig 17(b) and 17(c). These results highlight one of the key benefits of the GP-based approach, namely its ability to quantify the uncertainty associated with the traditional design profile and its flexibility to define bounds based on the desired risk level.

BENEFITS AND LIMITATIONS OF PROPOSED APPROACH

While significant advances have been made in prediction modelling, uncertainty surrounding the assessment of geotechnical parameters and underground conditions remains the main barrier to accurate prediction of construction behaviour (Jin et al. 2018). The observational method is desirable for its potential to save materials, time and costs relative to conventional design approaches (Spross and Johansson 2017). The proposed approach advances existing prescriptive design approaches for microtunnelling jacking forces by integrating the observational method within a Bayesian framework. Key advantages of this technique are that it provides (a) a robust approach for treating signal artefacts encountered in monitored construction data, (b) incorporates

uncertainty explicitly into the predictions and (c) the jacking distance-time-force relationship is allowed to adapt dynamically based on the latest information acquired during the drive. It also offers a means of quantifying the uncertainty associated with the traditional design profile and provides the flexibility of defining a probabilistic design profile based on the desired risk level. Furthermore, the model accounts for site-specific variations in slurry conditions, lubricant composition and delivery, and TBM driving style by influencing the monitored data (i.e. the jacking force-time-distance relationship).

It is worth noting that the methodology presented in this paper develops a probabilistic model of 'normality' based on the monitored data acquired at the time (i.e. the training data). The proposed approach is therefore not capable of forecasting features which are not present in the training data. For the case of unexpected events, such as sudden changes in ground conditions and drive trajectory, and encountering obstacles, the proposed approach can be used to detect deviations of the monitored data from normal working behaviour (i.e. 'anomaly detection'; see Sheil et al. (2020b) and Chieh et al. (2020) for additional information). It is also noteworthy that this methodology is applied on a *site-specific* basis; application of this technique *across* various sites is likely to necessitate a higher dimensional input dataset.

CONCLUDING REMARKS

This paper has described a probabilistic observational approach to forecast jacking forces during microtunnelling using Gaussian Process regression. The proposed approach was applied to two recent UK microtunnelling monitoring projects: Drive A was used to develop the forecasting methodology while Drive B was used for validation. The main conclusions from the study are as follows:

(a) Covariance functions were used to encode prior assumptions about the monitored data. The accuracy of 'short-term' forecasting was shown to be most closely linked to the 'smoothness of the covariance function; the best forecast accuracy was achieved using the Matérn 3/2 covariance function, followed by the Matérn 5/2 and squared exponential

covariance functions. The structure of the data, particularly stoppage-induced peaks in jacking force, was well-captured by the GP where all peaks in jacking force were encapsulated by a 99% prediction interval. This highlights the ability of the GP model to automatically establish a site-specific probabilistic relationship between stoppage time and jacking force.

(b) For 'long-term' forecasting, the best GP performance was achieved using a linear covariance function due to its simplified structure and its independence of a length-scale parameter. The much greater forecast horizon caused a significant increase in the uncertainty of the forecasts, and therefore the 99% prediction interval. While there is a clear deterioration in the fidelity of the GP's forecast of the distance-time-force relationship, the GP provides excellent forecasts of the linear friction trend in all instances.

(c) A 'computationally light' implementation of the proposed approach was explored by imposing a maximum size on the training dataset. Intuitively, smaller window sizes caused a gradual increase in error because of an insufficient amount of data to accurately describe the distance-time-force relationship. The results also suggest that long-term forecasting requires more data to reliably capture the long-term friction trend compared to short-term forecasting. Nevertheless, the results showed that the proposed approach can be optimised for real-time implementation for a modest trade-off in forecast accuracy.

(d) Rather than using a single upper bound estimate, the GP model was shown to provide an expedient means of deriving a probabilistic upper bound. For short-term forecasting, a 99% prediction interval is necessary to capture all jacking force peaks. Due to the increased uncertainty associated with long-term forecasting, it was shown that a 99% prediction interval is overly-conservative and even a 50% prediction interval provides a safe upper bound of the expected jacking forces.

(e) The proposed GP approach provided vastly improved predictions of monitored data from Drive B compared to design methods currently used in industry. Prescriptive design methods are not capable of capturing subtle site-specific variations in the construction process. These results also highlight one of the key benefits of the GP-based approach,

namely its ability to quantify the uncertainty associated with the traditional design profile and its flexibility to define a probabilistic design profile based on the desired risk level.

(f) The results of this study have revealed an exciting potential for probabilistic data-driven methods to complement existing jacking force design methods. It should also be noted that the results presented in this paper pertain to specific TBM/tunnel geometries and soil/lubrication conditions. Further validation and development of the proposed approach for application to more complex scenarios involving curved drives in mixed ground conditions is clearly desirable.

ACKNOWLEDGEMENTS

This research is supported by the Royal Academy of Engineering under the Research Fellowship Scheme.

REFERENCES

Barla, M., M. Camusso, and S. Aiassa. 2006. “Analysis of jacking forces during microtunnelling in limestone.” *Tunnelling and Underground Space Technology* 21 (6): 668-683. https://doi.org/10.1016/j.tust.2006.01.002.

Bergeson, W. 2014. “Review of long drive microtunneling technology for use on large scale projects.” *Tunnelling and Underground Space Technology* 39: 66-72. https://doi.org/10.1016/j.tust.2013.02.001

Chapman, D. N. and Y. Ichioka. 1999. “Prediction of jacking forces for microtunnelling operations.” *Tunnelling and Underground Space Technology* 14 (1): 31-41. https://doi.org/10.1016/S0886-7798(99)00019-X

Cheng, W. C., J. C. Ni, J. S. L. Shen, and H. W. Huang. 2017. “Investigation into factors affecting jacking force: a case study.” *Proceedings of the Institution of Civil Engineers-Geotechnical Engineering* 170 (4): 322-334. https://doi.org/10.1680/jgeen.16.00117

Chieh, W.-C., Bai, X.-D., Sheil, B.B. , Li, G. & Wang, F. (2020) Identifying characteristics of pipejacking parameters to assess geological conditions using optimisation algorithm-based support vector machines. *Tunnelling & Underground Space Technology.* Accepted.

Choo, C. S. and. E. L. Ong. 2015. “Evaluation of pipe-jacking forces based on direct shear testing of reconstituted tunneling rock spoils.” *Journal of Geotechnical and Geoenvironmental Engineering* 141 (10): 04015044. https://doi.org/10.1061/(ASCE)GT.1943-5606.0001348

CPAA. 2013. *Jacking Design Guidelines.* Concrete Pipe Association of Australasia.

Duvenaud, D., 2014. *Automatic model construction with Gaussian processes*. Doctoral dissertation, University of Cambridge.

Holliday, J. R., K. Z. Nanjo, K. F. Tiampo, J. B. Rundle, and D. L. Turcotte. 2005. "Earthquake forecasting and its verification." *arXiv preprint cond-mat/0508476*.

Japan Micro Tunneling Association, 2000. *Pipe-jacking Application*. JMTA, Tokyo.

Jin, Y., Biscontin, G. and Gardoni, P., 2018. A Bayesian definition of 'most probable' parameters. *Geotechnical Research*, *5*(3), pp.130-142.

Kim, K. J. 2003. "Financial time series forecasting using support vector machines." *Neurocomputing* 55 (1-2): 307-319. https://doi.org/10.1016/S0925-2312(03)00372-2

Matérn, B. *Spatial Variation.* Springer, New York, 1960.

Meskele, T. and A. W. Stuedlein. 2015. "Static soil resistance to pipe ramming in granular soils." *Journal of Geotechnical and Geoenvironmental Engineering* 141 (3): 04014108. https://doi.org/10.1061/(ASCE)GT.1943-5606.0001237

Milligan, G. W. E., and M. A. Marshall. 1998. "The functions and effects of lubrication in pipe jacking." *Tunnels and Metropolises, Negro Jr. and Ferreira (eds.), Balkema, Rotterdam* 2: 739-744.

Milligan, G. W. E., and P. Norris. 1999. "Pipe–soil interaction during pipe jacking." *Proceedings of the Institution of Civil Engineers-Geotechnical Engineering* 137 (1): 27-44. https://doi.org/10.1680/gt.1999.370104.

Norris, P. and G. W. E. Milligan. 1992. "Frictional resistance of jacked concrete pipes at full scale." In *Proceedings of International Conference on Trenchless Construction,* No-Dig*,* 92: 121-128.

O'Dwyer, K. G., B. A. McCabe, B. B. Sheil, and D. P. Hernon. 2018. "Blackpool South Strategy project: analysis of pipe-jacking records." In *Proceedings of Civil Engineering Research in Ireland (CERI 2018)*, CERI: Ireland.

O'Dwyer, K. G., B. A. McCabe, and B. B. Sheil. (2019) "Interpretation of pipe-jacking and lubrication records for drives in silty soil." *Underground Space*. https://doi.org/10.1016/j.undsp.2019.04.001.

Peck, R. B. 1969. "Advantages and limitations of the observational method in applied soil mechanics." *Geotechnique* 19 (2): 171-187. https://doi.org/10.1680/geot.1969.19.2.171.

Pedregosa, F., G. Varoquaux, A. Gramfort, et al. 2011. "Scikit-learn: Machine learning in Python." *Journal of Machine Learning Research*, 12: 2825-2830.

Pellet-Beaucour, A. L., and R. Kastner. 2002. "Experimental and analytical study of friction forces during microtunneling operations." *Tunnelling and Underground Space Technology* 17 (1): 83-97. https://doi.org/10.1016/S0886-7798(01)00044-X.

Phillips, B. M., R. Royston, B. B. Sheil, and B. W. Byrne. 2019. “Instrumentation and monitoring of a concrete jacking pipe.” In *Proceedings of the International Conference for Smart Infrastructure and Construction, Cambridge, UK*.

PJA 1995. “Guide to best practice for the installation of pipe jacks and microtunnels.” *Pipe Jacking Association, London*.

Rahjoo, S., M. Najafi, R. Williammee, and G. Khankarli. 2012. Comparison of jacking load models for trenchless pipe jacking. In *Pipelines 2012: Innovations in Design, Construction, Operations, and Maintenance, Doing More with Less*, 1507-1520.

Rasmussen, C. E., and C. K. Williams. 2006. *Gaussian processes for machine learning, 2*(3):4. Cambridge, MA: MIT Press.

Reilly, C. C., and T. L. Orr, T.L. 2012. “Analysis of interface friction effects on microtunnel jacking forces in coarse-grained soils.” In *Proceedings of the Bridge and Concrete Research in Ireland Conference*, 121-126.

Reis, B. Y., and K. D. Mandl. 2003. “Time series modeling for syndromic surveillance.” *BMC Medical Informatics and Decision Making* 3 (1): 2. https://doi.org/10.1186/1472-6947-3-2.

Royston, R., B. B. Sheil, and B. W. Byrne. 2020a. “Monitoring the construction of a large-diameter caisson in sand.” *Proceedings of the ICE – Geotechnical Engineering*. https://doi.org/10.1680/jgeen.19.00266.

Royston, R., Sheil, B.B. & Byrne, B.W. 2020b. “Undrained bearing capacity of the cutting face of large-diameter caissons.” *Géotechnique.* In Press.

Sheil, B. B., B. G. Curran, and B. A. McCabe. 2016. “Experiences of utility microtunnelling in Irish limestone, mudstone and sandstone rock.” *Tunnelling and Underground Space Technology* 51: 326-337. https://doi.org/10.1016/j.tust.2015.10.019.

Sheil, B.B., Suryasentana, S.K., Mooney, M.A. & Zhu, H. 2020a. “Machine learning to inform tunnelling operations: recent advances and future trends.” *Proceedings of the ICE - Smart Infrastructure and Construction.* In Press.

Sheil, B. B., S. K. Suryasentana, and W. C. Cheng. 2020b. “An assessment of anomaly detection methods applied to microtunnelling.” *Journal of Geotechnical and Geoenvironmental Engineering.* https://doi.org/10.1061/(ASCE)GT.1943-5606.0002326.

Shen, S. L., Q. L. Cui, C. E. Ho, and Y. S. Xu. 2016. “Ground response to multiple parallel microtunneling operations in cemented silty clay and sand.” *Journal of Geotechnical and Geoenvironmental Engineering* 142 (5): 04016001. https://doi.org/10.1061/(ASCE)GT.1943-5606.0001441.

Shi, P., W. Liu, J. Pan, and C. Yu. 2018. “Experimental and analytical study of jacking load during microtunneling Gongbei tunnel pipe roof.” *Journal of Geotechnical and Geoenvironmental Engineering*, 144 (1): 05017006. https://doi.org/10.1061/(ASCE)GT.1943-5606.0001801.

519 Shou, K., J. Yen, and M. Liu. 2010. “On the frictional property of lubricants and its impact on
520 jacking force and soil–pipe interaction of pipe-jacking.” *Tunnelling and Underground Space*
521 *Technology* 25 (4): 469-477. https://doi.org/10.1016/j.tust.2010.02.009.
522 Sofianos, A. I., P. Loukas, and C. Chantzakos. 2004. “Pipe jacking a sewer under
523 Athens.” *Tunnelling and underground space technology* 19 (2): 193-203.
524 https://doi.org/10.1016/S0886-7798(03)00108-1.
525 Spross, J., and F. Johansson. 2017. “When is the observational method in geotechnical
526 engineering favourable?.” *Structural safety* 66: 17-26.
527 https://doi.org/10.1016/j.strusafe.2017.01.006.
528 Staheli, K. 2006. *Jacking force prediction: An interface friction approach based on pipe surface*
529 *roughness*. Doctoral dissertation, Georgia Institute of Technology.
530 Stroud, M. A. 1989. The Standard Penetration Test – its application and interpretation. In
531 *Proceedings of the ICE Conference on Penetration Testing in the UK*, Thomas Telford,
532 London.
533 Sun, Y., F. Wu, W. Sun, H. Li, and G. Shao. 2019. “Two Underground Pedestrian Passages Using
534 Pipe Jacking: Case Study.” *Journal of Geotechnical and Geoenvironmental*
535 *Engineering* 145 (2): 05018004. https://doi.org/10.1061/(ASCE)GT.1943-5606.0002006

Table 1 List of core covariance functions including their specific hyperparameters and formulation

Covariance function	Hyperparameters	Formulation
Linear, k_{LIN}	Output variance, σ^2, inhomogeneity factor, σ_0^2	$\sigma^2(\sigma_0^2 + < x, x' >)$
Periodic, k_{PER}	Output variance, σ^2, length-scale, l, and period p	$\sigma^2 \exp\left(-2\frac{sin^2\left(\frac{\pi}{p}\lvert x - x'\rvert\right)}{l^2}\right)$
Squared exponential, k_{SE}	Output variance, σ^2, length-scale, l	$\sigma^2 \exp\left(-\frac{(x-x')^2}{2l^2}\right)$
Matérn 5/2, k_{MAT5}	Output variance, σ^2, and length-scale, l. Smoothness parameter, v = 5/2 (fixed)	$\sigma^2\left(1+\frac{\sqrt{5}r}{l}+\frac{5r^2}{3l^2}\right)\exp\left(-\frac{\sqrt{5}r}{l}\right)$ where $r = \sqrt{(x-x')^T(x-x')}$
Matérn 3/2, k_{MAT3}	Output variance, σ^2, and length-scale, l. Smoothness parameter, v = 3/2 (fixed)	$\sigma^2\left(1+\frac{\sqrt{3}r}{l}\right)\exp\left(-\frac{\sqrt{3}r}{l}\right)$

Table 2 Optimal covariance functions and training window size composition for all four levels of forecasting

Forecast horizon	Covariance function structure	Maximum size of training window, *r*
Short-term; *h* = 1 (0.2 m)	$k_{MAT3+MAT5}$	250 (50 m)
Medium-term; *h* = 12 (2.4 m)	k_{LIN+SE}	250 (50 m)
Medium-term; *h* = 50 (10 m)	k_{LIN}	500 (100 m)
Long-term; variable *h*	k_{LIN}	500 (100 m)

Table 3 Jacking resistance recommendations according to the CPAA (2013) design guidelines

Ground condition	Jacking resistance per unit surface area (kPa)
Rock	2 − 3
Boulder clay	5 – 18
Firm clay	5 – 20
Wet clay	10 – 15
Silt	5 − 20
Dry loose sand	25 − 45

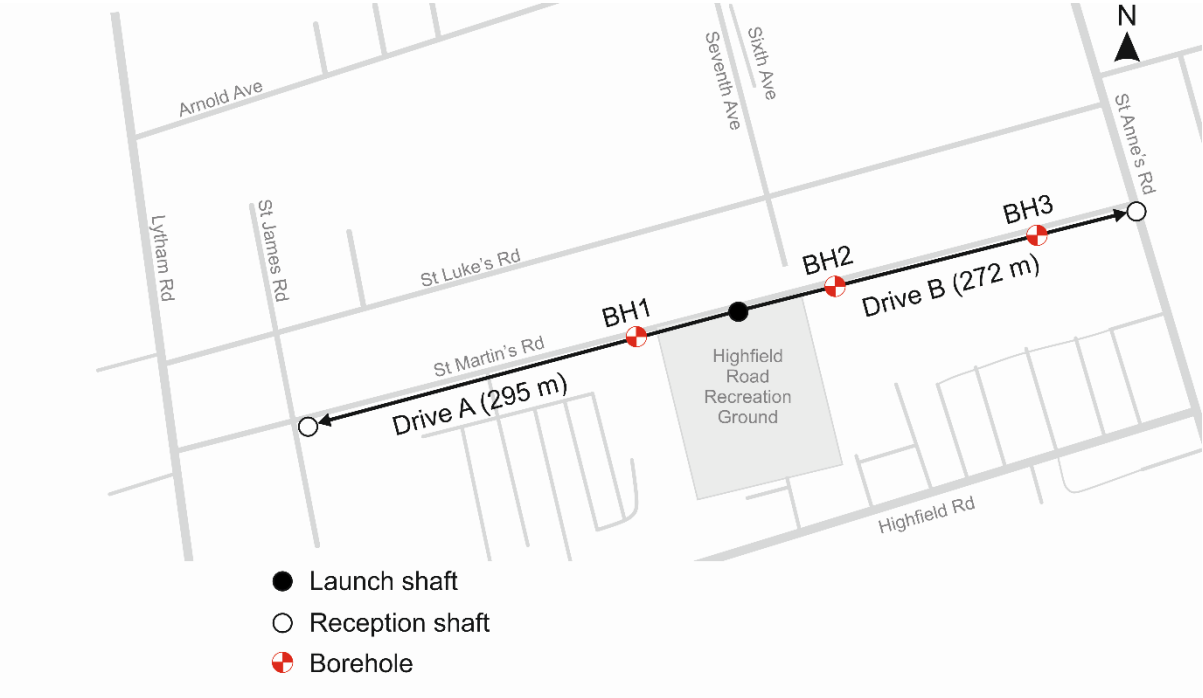

Fig. 1 Location of tunnels and shafts for Drives A and B at the Blackpool site

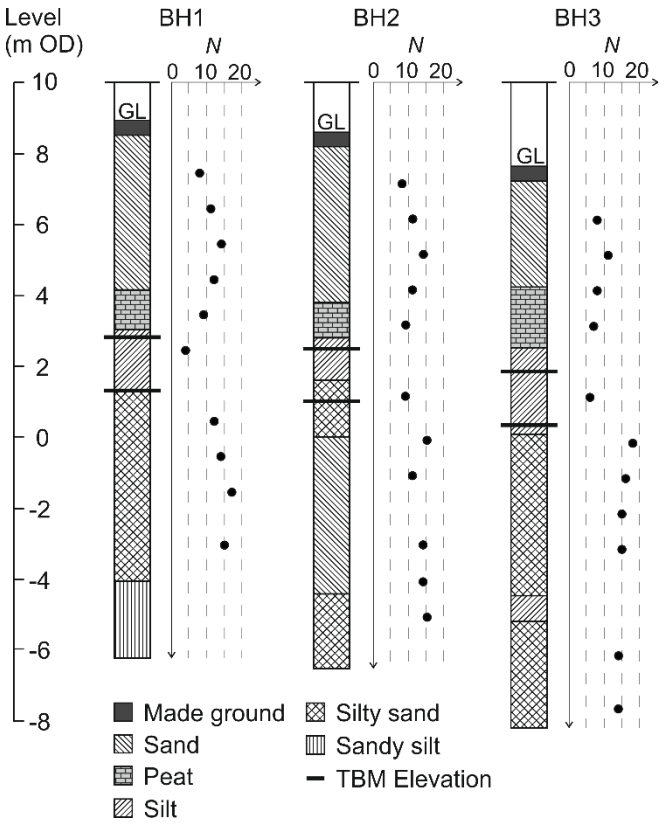

Fig. 2 Stratigraphy at the boreholes along the tunnel drive as well as the associated uncorrected SPT profiles

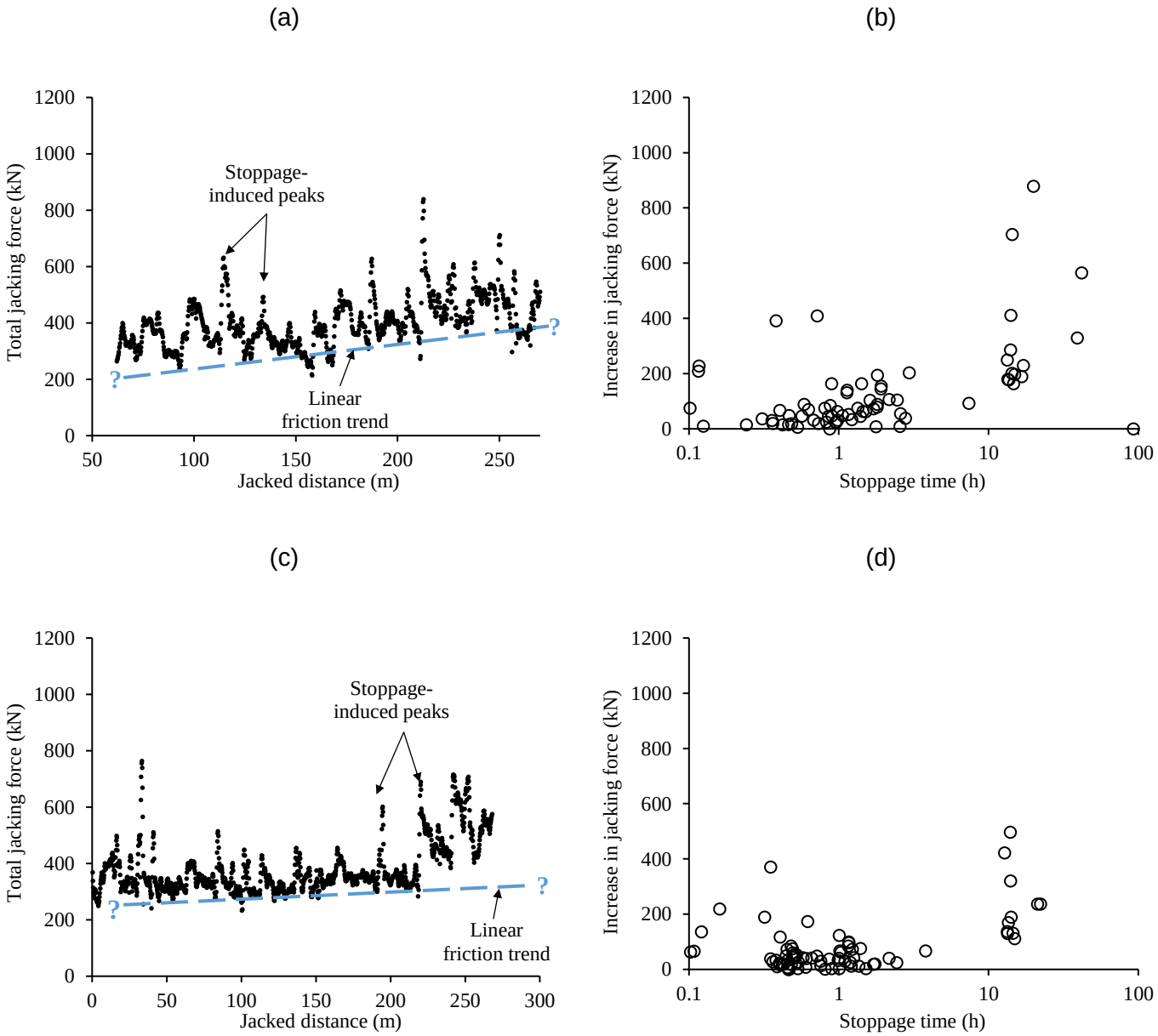

Fig. 3 Monitored data acquired from TBM records showing relationship between (a) total jacking force and jacked distance for Drive A, (b) stoppage time and increase in jacking force for Drive A, (c) total jacking force and jacked distance for Drive B, (d) stoppage time and increase in jacking force for Drive B

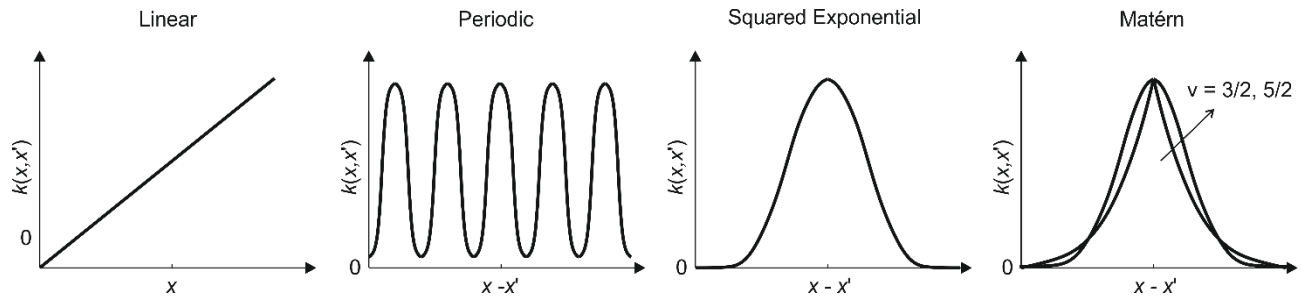

Fig. 4 Illustrations of the structure of the five 'core' covariance functions adopted in this study

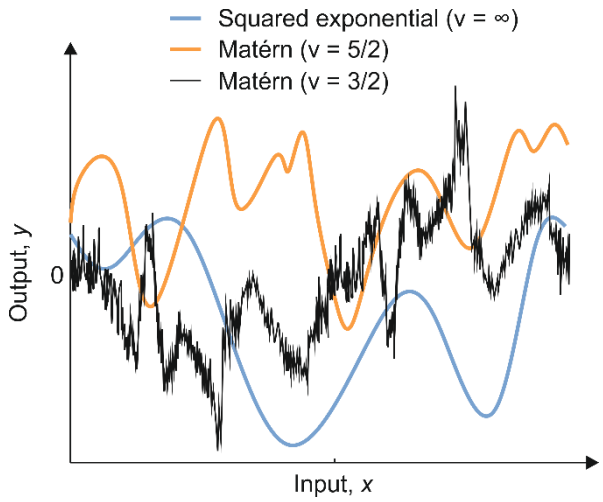

Fig. 5 Illustration of functions randomly drawn from a GP with squared exponential and Matérn covariance functions for different values of v.

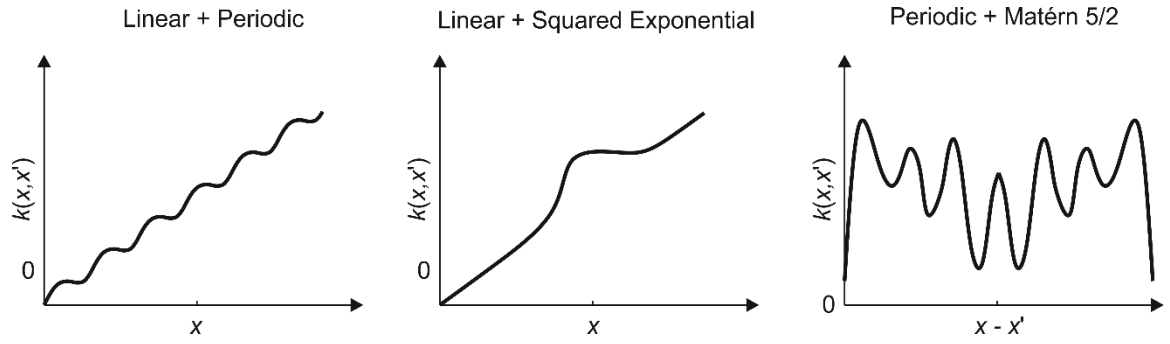

Fig. 6 Illustrations of the structure of covariance functions developed by summing various pairs of the core covariance functions considered in this paper.

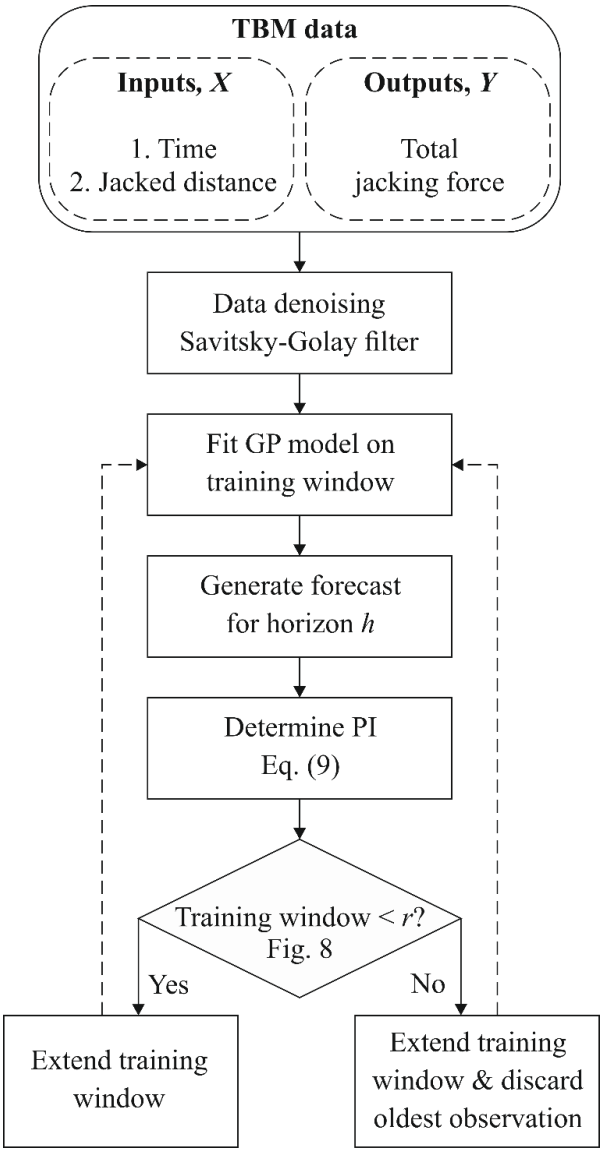

Fig. 7 Implementation of the proposed forecasting strategy

(a)

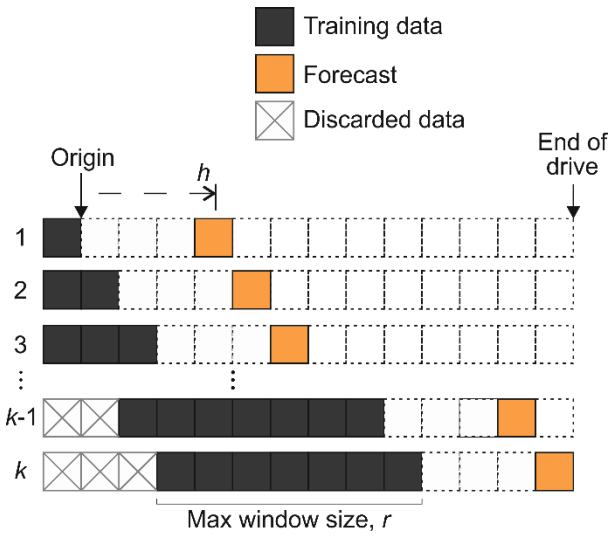

(b)

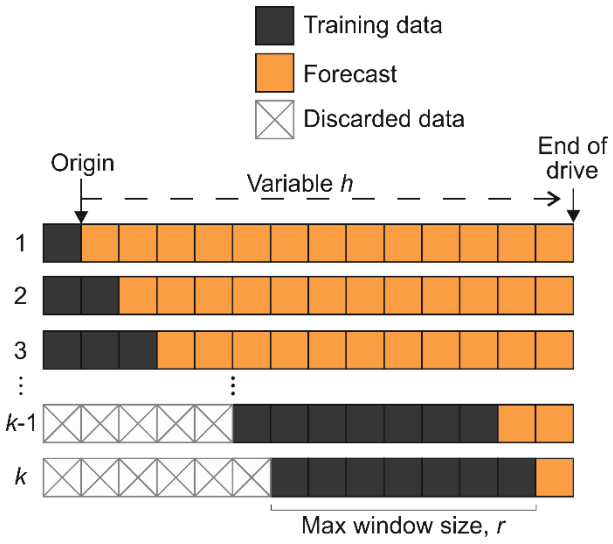

Fig. 8 Illustration of sliding window approach for (a) forecasting *h* steps ahead and (b) 'long-term' forecasting

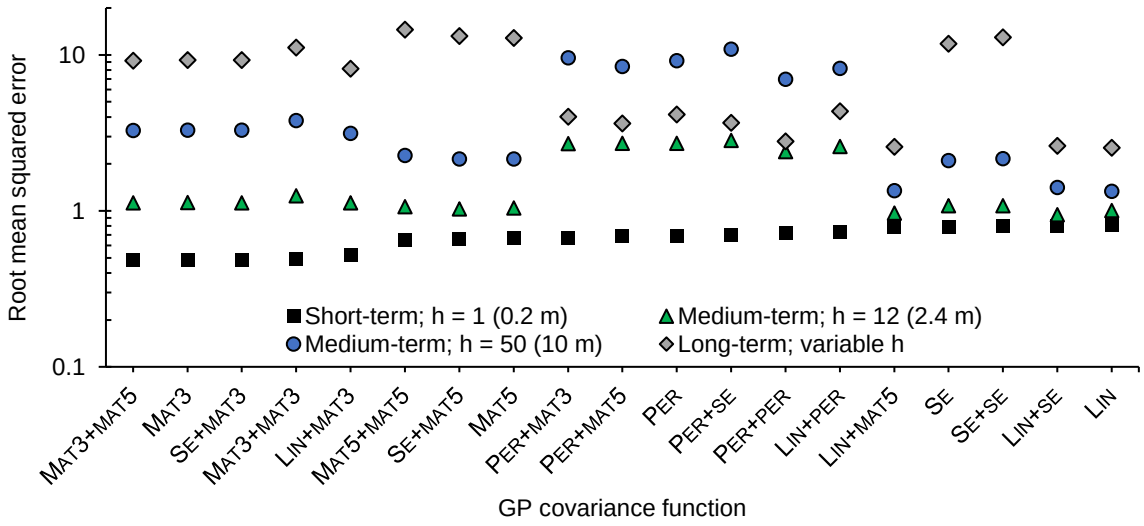

Fig. 9 GP forecasting results using the RMSE defined in equation (10) for all 19 instances of the covariance function and for four different forecast horizons: h = 1 (0.2 m; 'short-term'), h = 12 and 50 (2.4 m and 10 m; 'medium-term'), and long-term (variable h); Drive A, $r = \infty$.

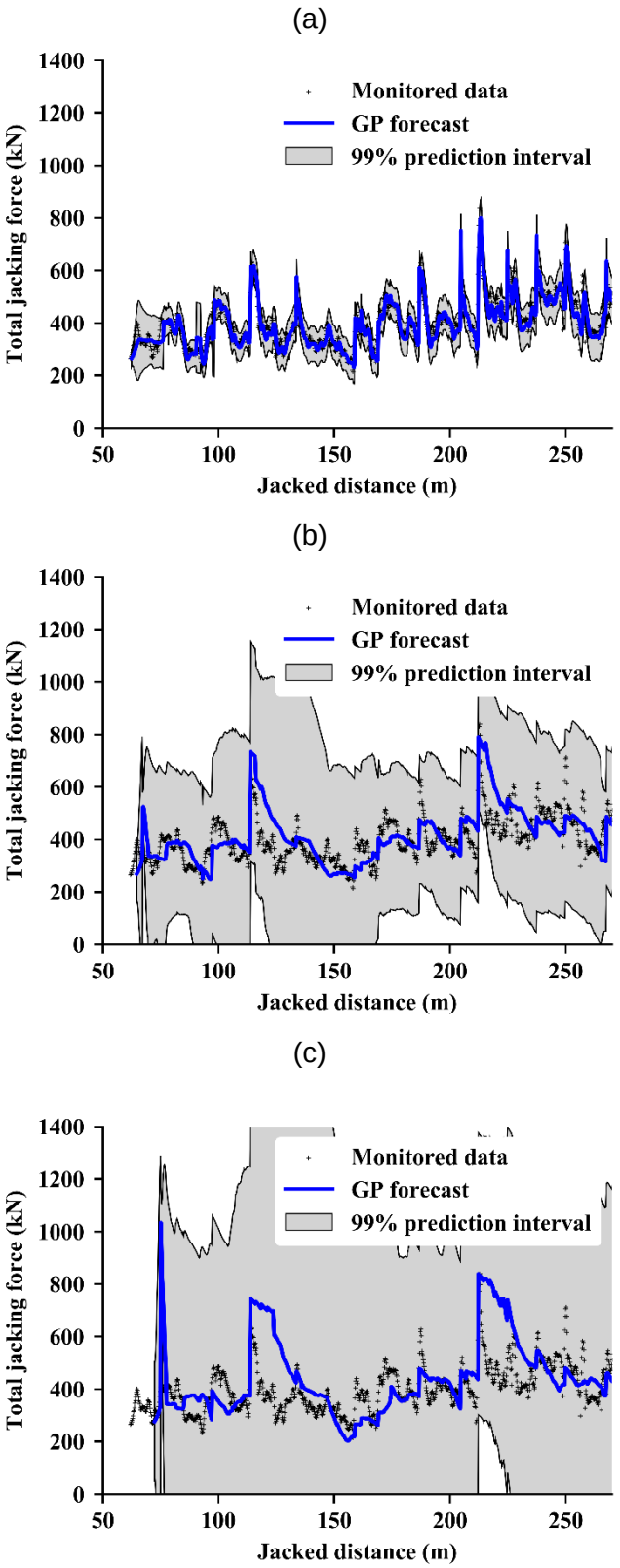

Fig. 10 Short- and medium-term forecasts of the development of total jacking force with jacked distance using the most accurate GP covariance functions compared to the Drive A monitored data: (a) h = 1 (0.2 m) using $k_{MAT3+MAT5}$, (b) h = 12 (2.4 m) using k_{LIN+SE}, (c) h = 50 (10 m) using $k_{LIN;}$ $r = \infty$

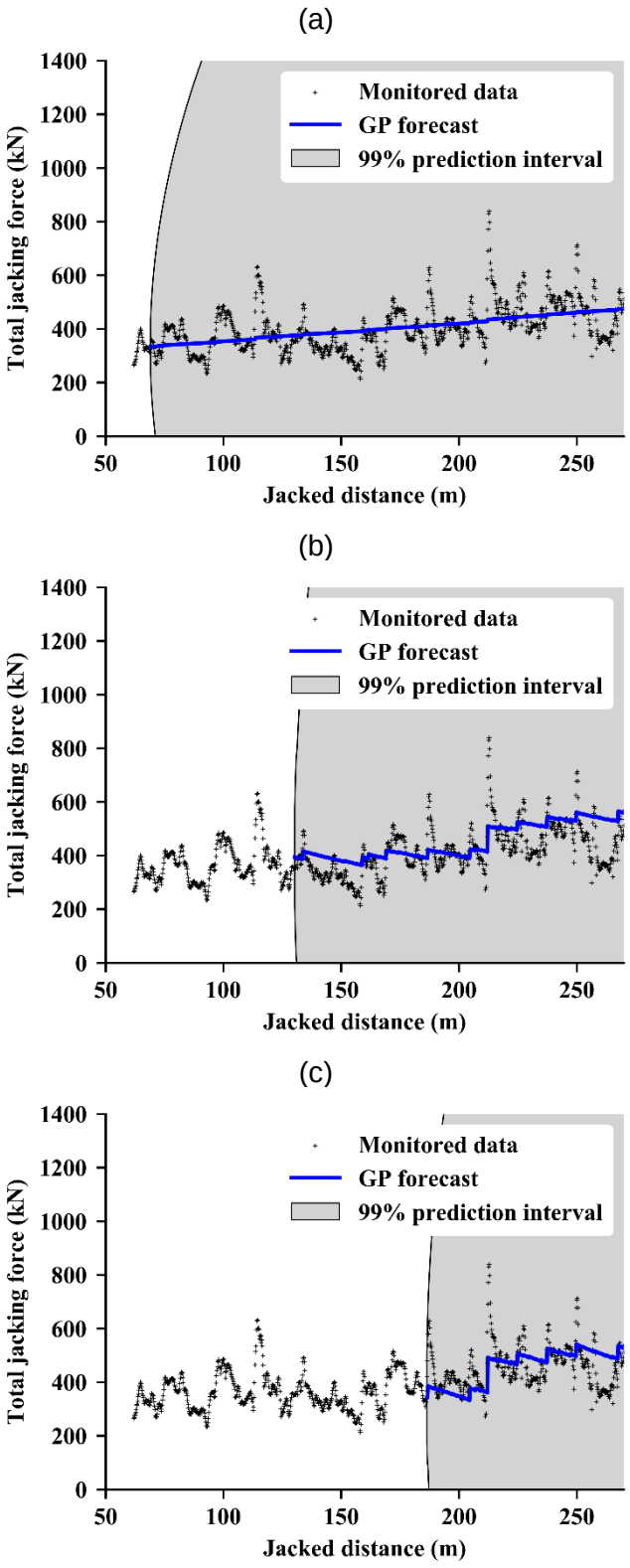

Fig. 11 Long-term forecasts of the development of total jacking force with jacked distance using the best-performing GP covariance function (k_{LIN}) compared to the Drive A monitored data for forecast origins of (a) 69 m (k = 35), (b) 130 m (k = 340), (c) 192 m (k = 650) where k is defined in Fig. 8(b); $r = \infty$

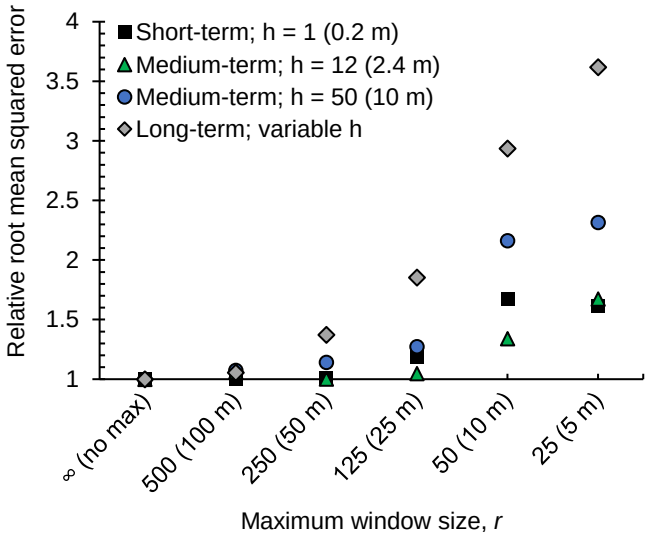

Fig. 12 Influence of the maximum window size, *r*, on the accuracy of GP forecasts using the RMSE relative to the corresponding r = ∞ value for four different forecast horizons; Drive A

(a)

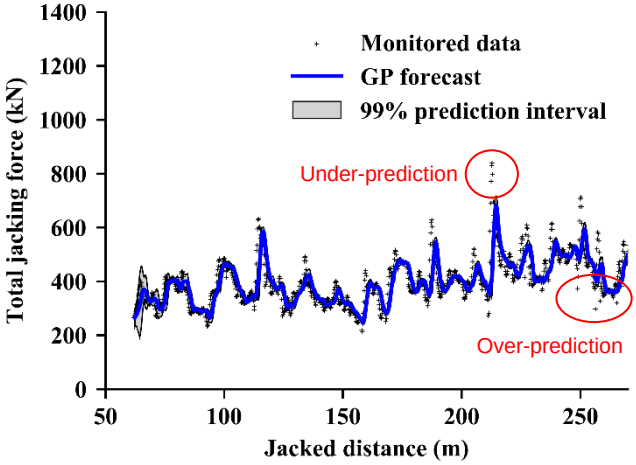

(b)

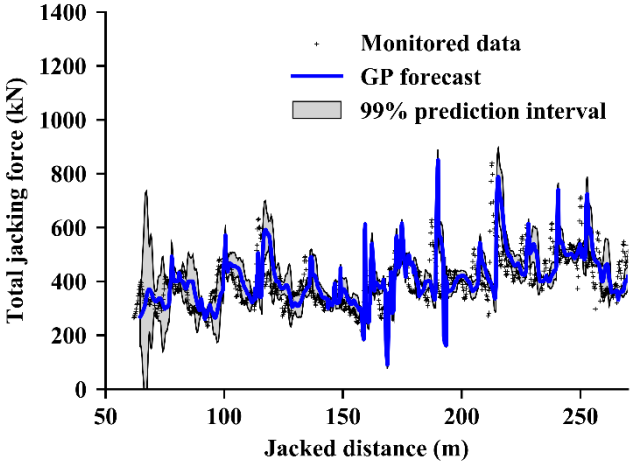

(c)

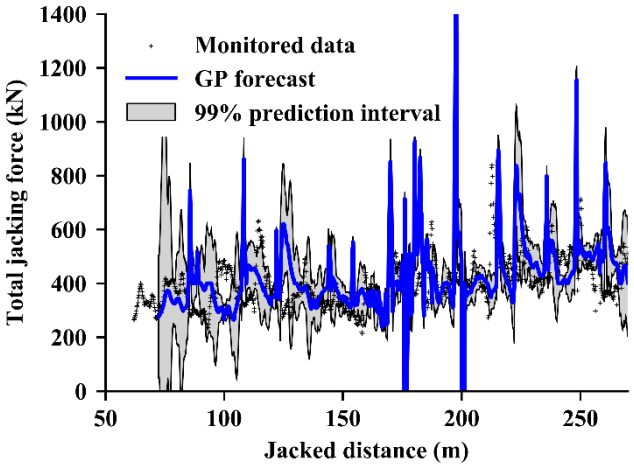

Fig. 13 Short- and medium-term forecasts of the development of total jacking force with jacked distance using the most accurate GP covariance functions with r = 12 (2.4 m) compared to the Drive A monitored data: (a) h = 1 (0.2 m) using $k_{MAT3+MAT5}$, (b) h = 12 (2.4 m) using k_{LIN+SE}, (c) h = 50 (10 m) using k_{LIN}.

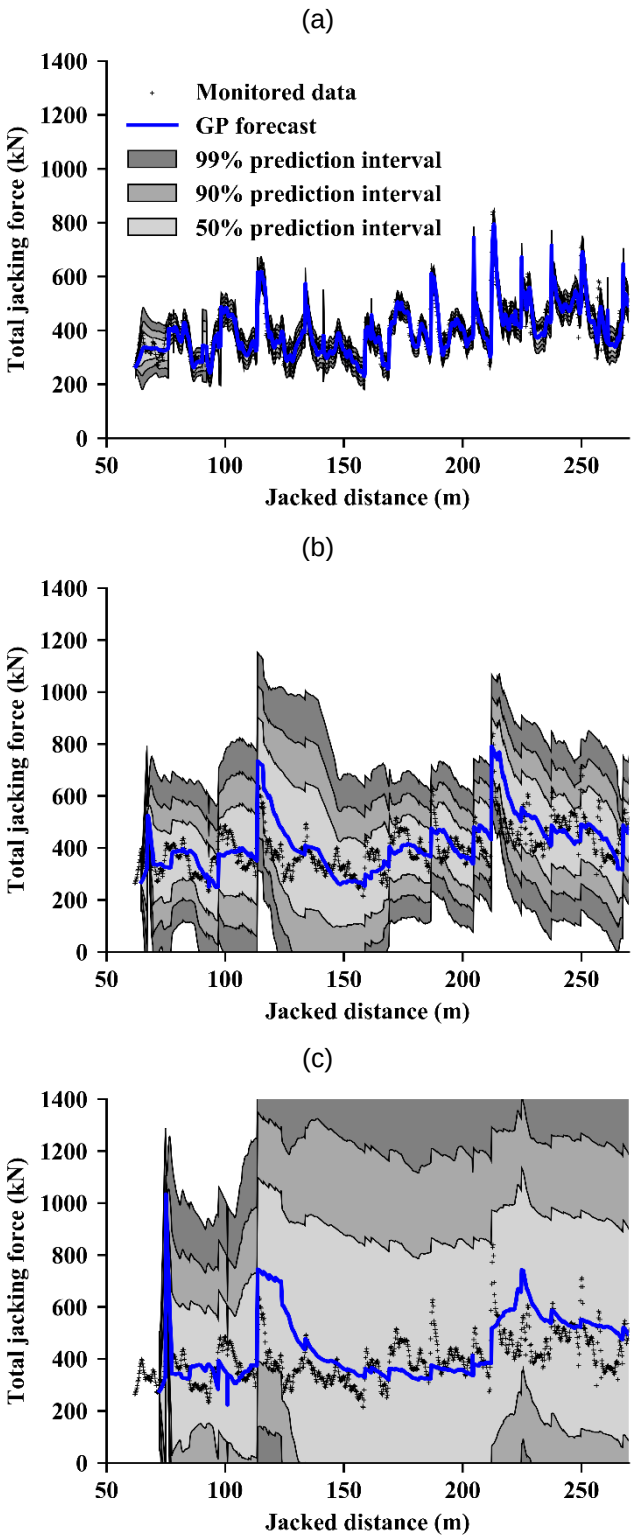

Fig. 14 Influence of prediction interval on short- and medium-term forecasts of maximum jacking forces using the 'optimal parameters' presented in Table 2 and compared to the Drive A monitored data: (a) h = 1 (0.2 m) using $k_{MAT3+MAT5}$ and r = 250, (b) h = 12 (2.5 m) using k_{LIN+SE} and r = 250, (c) h = 50 (10 m) using k_{LIN} and r = 500

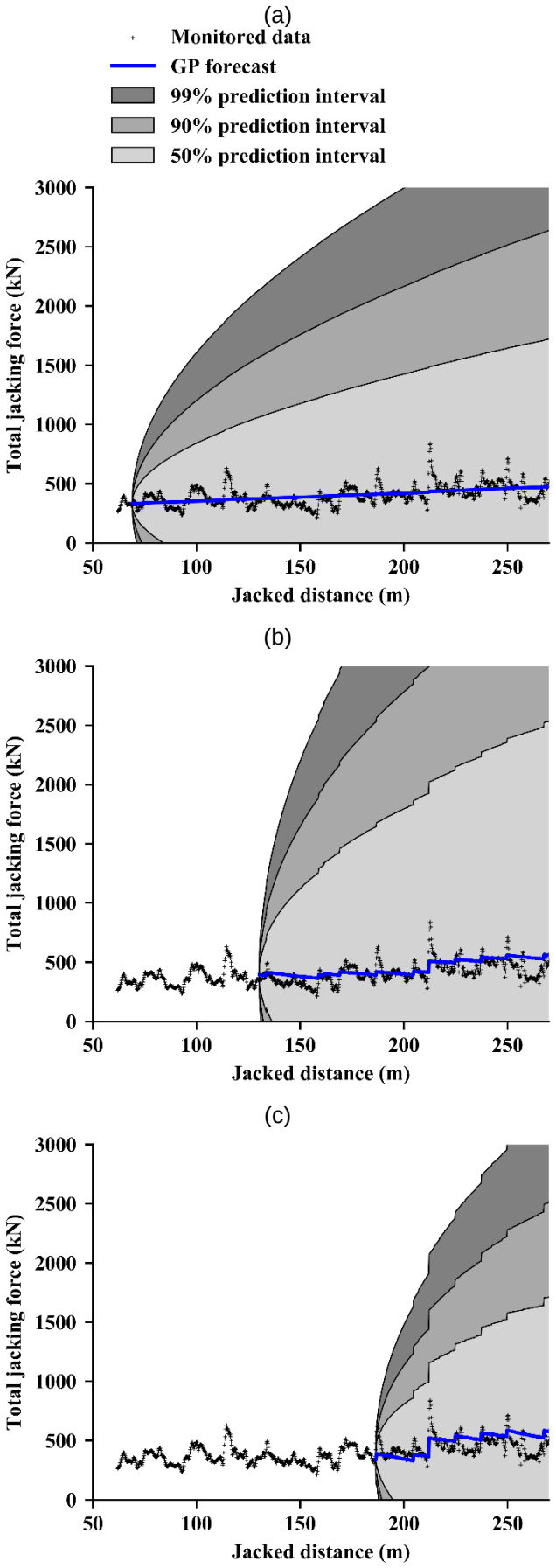

Fig. 15 Long-term forecasts of the development of total jacking force with jacked distance using the best-performing GP covariance function (k_{LIN}) compared to the Drive A monitored data for forecast origins of (a) 69 m (k = 35), (b) 130 m (k = 340), (c) 192 m (k = 650) where k is defined in Fig. 8(b)

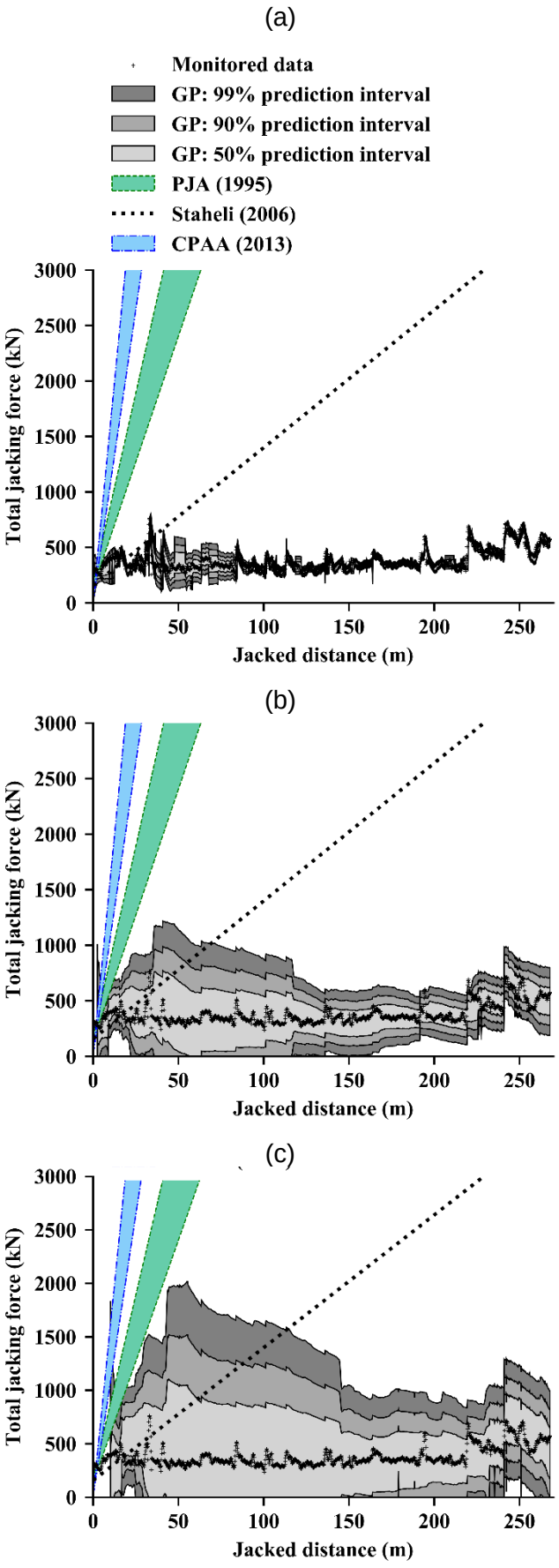

Fig. 16 Comparison of short- and medium-term GP forecasts of Drive B jacking forces with predictions determined using existing design methods: (a) h = 1 (0.2 m) using $k_{MAT3+MAT5}$ and r = 250, (b) h = 12 (2.5 m) using k_{LIN+SE} and r = 250, (c) h = 50 (10 m) using k_{LIN} and r = 500

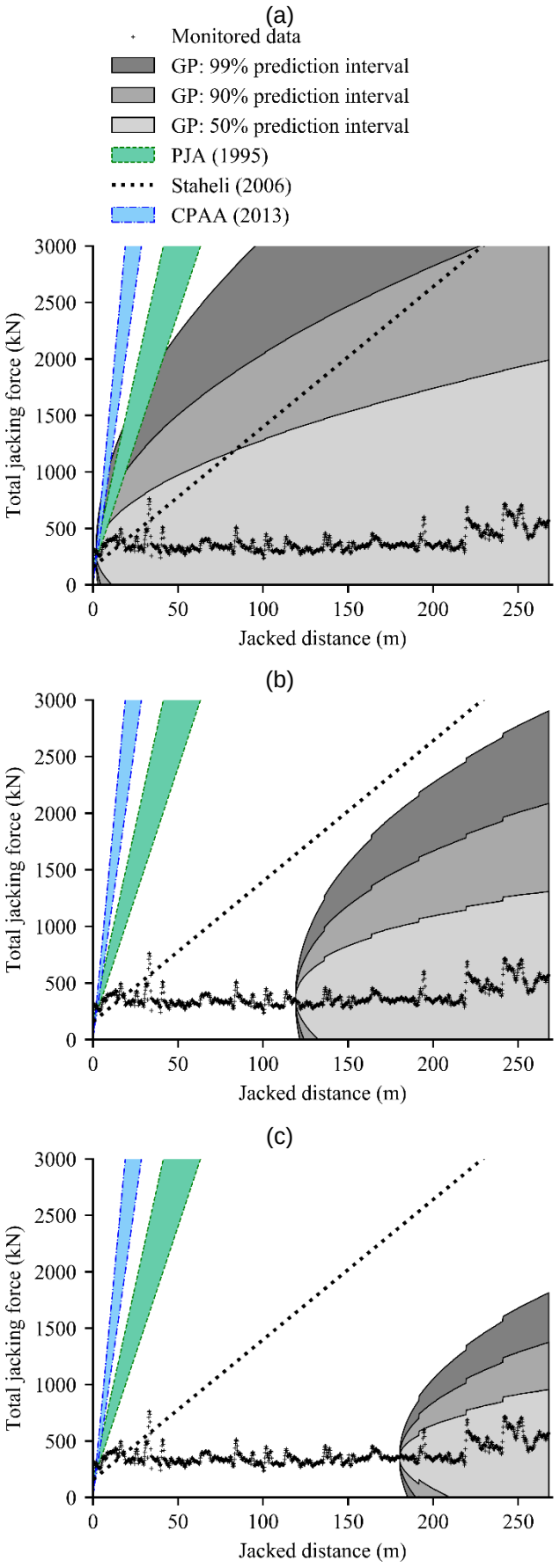

Fig. 17 Comparison of long-term GP forecasts of Drive B jacking forces with predictions determined using existing design guidelines for forecast origins of (a) 2 m (k = 10), (b) 117 m (k = 585), (c) 177 m (k = 885) where k is defined in Fig. 8(b)